



## Viscosity of magmatic liquids: A model

Daniele Giordano <sup>a,\*</sup>, James K. Russell <sup>b</sup>, Donald B. Dingwell <sup>c</sup>

<sup>a</sup> Department of Geological Sciences, Third University of Rome, Largo S. Leonardo Murialdo 1, 00154 Rome, Italy

<sup>b</sup> Volcanology & Petrology Laboratory, Earth and Ocean Sciences, University of British Columbia, Vancouver, Canada V6T 1Z4

<sup>c</sup> Earth and Environmental Sciences, University of Munich, Theresienstr. 41/III, 80333 Munich, Germany

### ARTICLE INFO

#### Article history:

Received 7 August 2007

Received in revised form 19 March 2008

Accepted 27 March 2008

Available online 9 April 2008

Editor: C.P. Jaupart

#### Keywords:

viscosity  
model  
silicate-melts  
volatile-bearing-melts  
glass transition  
fragility

### ABSTRACT

The viscosity of silicate melts controls magma transport dynamics, eruption style and rates of physicochemical processes (e.g., degassing, crystallization) in natural magmas. Thus a comprehensive viscosity model for magmatic liquids has long been a goal of earth scientists. Here we present a model that predicts the non-Arrhenian Newtonian viscosity of silicate melts as a function of T and melt composition, including the rheologically important volatile constituents H<sub>2</sub>O and F. Our model is based on > 1770 measurements of viscosity on multicomponent anhydrous and volatile-rich silicate melts. The non-Arrhenian T-dependence of viscosity is accounted for by the VFT equation [ $\log \eta = A + B / (T(K) - C)$ ]. The optimization assumes a common, high-T limit (A) for silicate melt viscosity and returns a value for this limit of  $-4.55 (+0.2)$  (e.g.,  $\log \eta \sim 10^{-4.6}$  Pa s). All compositional dependence is ascribed to the parameters B and C and is accounted for by an additional 17 model coefficients. Our model is continuous in composition- and temperature-space and predicts the viscosity of natural volatile-bearing silicate melts (SiO<sub>2</sub>, Al<sub>2</sub>O<sub>3</sub>, TiO<sub>2</sub>, FeO<sub>tot</sub>, CaO, MgO, MnO, Na<sub>2</sub>O, K<sub>2</sub>O, P<sub>2</sub>O<sub>5</sub>, H<sub>2</sub>O, F<sub>2</sub>O<sub>-1</sub>) over fifteen log units of viscosity ( $10^{-1} - 10^{14}$  Pa s). The model for viscosity can also predict other transport properties including glass transition temperatures ( $T_g$ ) and melt fragility ( $m$ ). We show strong systematic decreases in  $T_g$  and  $m$  with increasing volatile content. This pattern has implications for predicting styles of volcanic eruption and understanding silicate melt structure. Our model transforms a quarter-century of experimental study of melt viscosities, into a parameterisation having a predictive capacity that makes it relevant to diverse fields of research including: volcanology, geophysics, petrology and material sciences.

© 2008 Elsevier B.V. All rights reserved.

### 1. Introduction

Viscosity is the single most important physical property governing the production, transport and eruption of magmas (Papale, 1999; Sparks, 2004; Dingwell, 2006). The viscosity of naturally-occurring silicate magmas can span more than 15 orders of magnitude ( $10^{-1} - 10^{14}$  Pa s) primarily in response to variations in temperature (T), melt composition and the proportions of suspended solids and/or exsolved fluid phases (Dingwell, 1996; Giordano et al., 2004a,b). Dissolved volatiles, such as H<sub>2</sub>O (Giordano et al., 2004a) and F (Giordano et al., 2004b), are of particular importance because small variations in their concentrations can generate large ( $> 10^5$ ) and strongly nonlinear changes in melt viscosity that drastically affect magma transport, ascent and eruption dynamics. These effects may even dictate whether eruptions are effusive or explosive (Dingwell, 1996; Papale, 1999; Sparks, 2004). Other volatile components (CO<sub>2</sub>, Cl, Br, I, S) appear to be less important in terms of directly influencing viscosity (e.g., Dingwell and Hess, 1998; Bourgué and Richet, 2001; Zimova and Webb, 2006). Thus, the accurate prediction of silicate melt viscosity as a function of temperature and composition,

including H<sub>2</sub>O and F, is of paramount importance for modelling and understanding magmatic and volcanic processes.

The task of creating such models has been hampered, to date, by the complexity of incorporating these volatile effects, together with multicomponent melt compositional effects, into the framework of a non-Arrhenian model (Baker, 1996; Hess and Dingwell, 1996; Russell et al., 2002; Giordano and Dingwell, 2003; Russell and Giordano, 2005; Giordano et al., 2006; Vetere et al., 2006; Hui and Zhang, 2007). The earliest models for predicting the viscosity of geologically-relevant silicate melts adopted a strictly Arrhenian temperature dependence (Shaw, 1972; Bottinga and Weill, 1972). These models were based on a relatively small number of high-T experiments (~130). They were, and remain, quite effective in reproducing silicate melt viscosities over a restricted range of compositions at high, generally near-liquidus, temperatures. Arrhenian models, however, inevitably fail when extrapolated to lower temperatures. This is a simple consequence of the now universal observation that silicate melts show pronounced non-Arrhenian temperature dependence (Dingwell et al., 1993; Richet and Bottinga, 1995).

Accordingly, the next generation of viscosity models for silicate melts adopted a non-Arrhenian T-dependence usually involving 3 (rather than 2) adjustable parameters. These models were, however, designed to span restricted ranges in melt composition and some are extremely effective in doing so. For example, several of these

\* Corresponding author. Tel.: +39 06 54888018, +39 339 1315725; fax: +39 050 552085.

E-mail address: [dgiordano@uniroma3.it](mailto:dgiordano@uniroma3.it) (D. Giordano).

computational schemes were developed to model the effects of H<sub>2</sub>O on the viscosity of single specific melt composition (Baker, 1996; Hess and Dingwell, 1996; Giordano et al., 2004a; Vetere et al., 2006). There are several models for melt viscosity that incorporate a non-Arrhenian T-dependence and span wide ranges of melt composition (e.g., Giordano and Dingwell, 2003; Russell and Giordano, 2005; Giordano et al., 2006). However, they do not incorporate the effects of dissolved volatiles (especially H<sub>2</sub>O and F). The sole exception is the model published by Hui and Zhang (2007) which predicts melt viscosity as a function of temperature and composition and is applicable to hydrous silicate melts. Currently, this is the only viscosity model for multi-component silicate melts that accounts for the effects of H<sub>2</sub>O.

Here we present a multicomponent chemical model for predicting the viscosity of naturally-occurring silicate melts based on experimental measurements of viscosity at T(K) on melts of known composition (Fig. 1) at atmospheric pressure (10<sup>5</sup> Pa). The model has

the following attributes: i) it spans most of the compositional range found in naturally-occurring volcanic rocks, ii) it captures the effects of 10 major and minor oxide components and the volatile components H<sub>2</sub>O and F, iii) it is computationally continuous across the entire compositional and temperature spectrum of the database, iv) it is capable of accommodating both *strong* (near-Arrhenian T-dependence) and *fragile* (non-Arrhenian T-dependence) behaviour of silicate melts (e.g., Angell, 1985), and v) it reproduces observed relationships between melt composition and transport properties such as glass transition temperature ( $T_g$ ) and fragility ( $m$ ) (Angell, 1985; Plazek and Ngai, 1991) (see Section 5.2 for definition).

We anticipate this model finding widespread use in the petrological and volcanological sciences because of these traits. In particular, the low number (i.e. 18) of model parameters should facilitate incorporation into complex applications (e.g., volcanic eruption models) that involve dynamic changes in melt composition and for greater stability when the model is extrapolated outside the compositional range of the experimental database.

## 2. Experimental database

The primary dataset, against which the model is calibrated, comprises 1774 experimentally measured pairs of values of T(K) and log  $\eta$  on silicate melts of known composition. Our database includes measurements from many laboratories but most are from work in experimental labs from the past 20 years; sources of data are available as supporting material in the Appendix. Most measurements derive from high-T concentric cylinder experimentation ( $\eta \sim 10^{-1}$  to  $10^5$  Pa s) and from micropenetration-dilatometric or parallel plate techniques for low-T ( $\eta \sim 10^8$  to  $10^{14}$  Pa s). By exploiting the relative differences in structural relaxation timescales and rates of crystallization and vesiculation at temperatures immediately above glass transition temperatures, the micropenetration and the parallel plate techniques can be used for viscosity measurements on both dry and hydrous silicate melts. The hydrous melts are synthesized at high-T and high-P conditions using conventional piston cylinder or hydrothermal bombs techniques (Giordano et al., 2004a,b; Dingwell, 2006; Vetere et al., 2006). The apparent gap in data between  $10^5$  Pa s and  $10^8$  Pa s results from a conflict between the timescales of melt relaxation (i.e., measurement) and timescales of processes that modify the material properties (i.e., crystallization and vesiculation).

The range of melt compositions in the database spans virtually all common terrestrial volcanic rocks: from basic to silicic, from subalkaline to peralkaline, and from metaluminous to peraluminous (Fig. 1). The total number of experiments used in this study is substantially larger than that used in previous analyses and represents virtually all published measurements of viscosity on multicomponent natural or natural equivalent silicate melts. We have elected not to include datasets from simple non-natural chemical systems (e.g., Russell and Giordano, 2005; Giordano and Russell, 2007).

The database for anhydrous melt compositions includes 932 measurements of viscosity on 58 melt compositions spanning a temperature range of 535–1705 °C (Fig. 2A). Measured values of viscosity are from  $10^{-1}$  to  $10^{13.8}$  Pa s. The calibration dataset also includes 842 measurements on volatile (H<sub>2</sub>O and F) enriched melts (Fig. 2B). These experiments commonly use the anhydrous melts as a base composition to which volatiles have been added. Including variations in volatile content (Fig. 1C), the 842 experiments are performed on 140 different melt compositions, and explore essentially the same range of viscosity values ( $10^{0.1}$  to  $10^{13.4}$  Pa s) but over a considerably lower range of experimental temperatures: 245–1580 °C (Fig. 2B).

The multicomponent model is calibrated on melt compositions spanning oxide contents (wt.%) of: SiO<sub>2</sub> (41–79), TiO<sub>2</sub> (0–3), Al<sub>2</sub>O<sub>3</sub> (0–23), FeO<sub>Tot</sub> (0–12), MnO (0–0.3), MgO (0–32), CaO (0–26), Na<sub>2</sub>O (0–11), K<sub>2</sub>O (0.3–9), P<sub>2</sub>O<sub>5</sub> (0–1.2). Dissolved volatile contents vary from about 0 to 8 wt.% H<sub>2</sub>O and 0 to 4 wt.% F (Fig. 1C). The base compositions (e.g., anhydrous) of the volatile-enriched melts span nearly the same

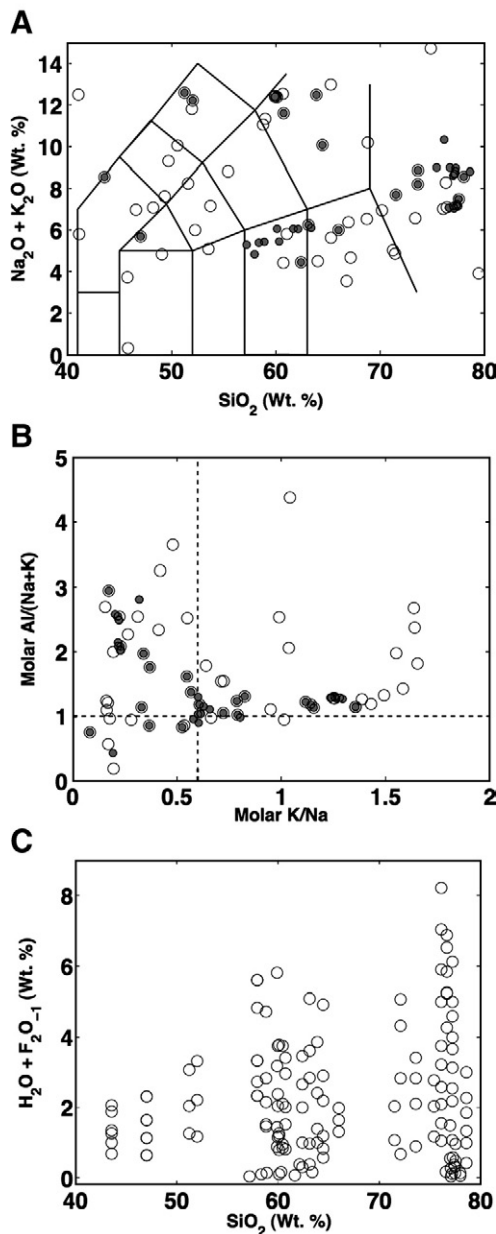
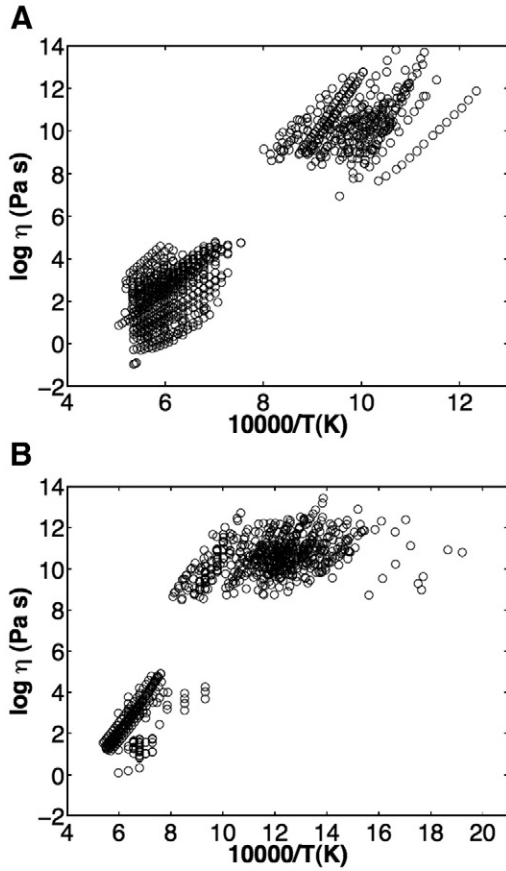


Fig. 1. Melt compositions used in calibration of model for silicate melt viscosity, including volatile-free (open circles) and volatile-enriched (H<sub>2</sub>O and F<sub>2</sub>O<sub>-1</sub>) melts. Melt compositions plotted as: (A) wt.% SiO<sub>2</sub> vs. Na<sub>2</sub>O + K<sub>2</sub>O, (B) molar ratios of K/Na vs. Al/(Na + K), and (C) wt.% SiO<sub>2</sub> vs. total volatile content.



**Fig. 2.** Summary of data used to calibrate VFT model for compositional dependence of silicate melt viscosity. Data shown as  $\log \eta$  vs.  $10,000/T(K)$  for (A) volatile-free, and (B) volatile-rich melts (Sources listed as supporting material in the Appendix). Note vertical axes are equivalent but horizontal axis for (B) has been extended to lower temperatures.

compositional range as the anhydrous dataset (Fig. 1A, B). In the present analysis the NBO/T parameter (number of non-bridging oxygens per tetrahedra), representing a first order approximation to the degree of polymerization of the melt, is calculated accordingly to Mysen (1988) by assuming that  $\text{SiO}_2$ ,  $\text{TiO}_2$ ,  $\text{Al}_2\text{O}_3$ , and  $\text{Fe}_2\text{O}_3$  are network formers. For the purposes of NBO/T calculations only, total iron ( $\text{FeO}_T$ ) was split equally (wt.%) between FeO and  $\text{Fe}_2\text{O}_3$  (Giordano and Dingwell, 2003; Giordano et al., 2006); calculated values of NBO/T for all melts in the database range from 0 to 1.8.

### 3. Model optimization

The experimental database comprises only viscosity measurements that are coupled to melts for which there are complete and accurate compositions, including direct analysis of volatiles (e.g., spectroscopic or volumetric). We use the oxide mol% as a chemical basis and treat all iron as FeO even though there is evidence that  $\text{Fe}_2\text{O}_3$  and FeO play distinct roles in governing melt structure (Mysen, 1988) and that the redox state of very Fe-rich melts does measurably influence viscosity (Dingwell, 1991). Our redox simplification here is purely empirical, resulting from the fact that tests for model improvement, based on a redox factor, fail to produce an improvement of the fit. Fluorine is treated as mol%  $\text{F}_2\text{O}_{-1}$  (Giordano et al., 2004b).

Temperature dependence of viscosity ( $\eta$ ) is modelled by the VFT equation (Vogel, 1921; Fulcher, 1925):

$$\log \eta = A + \frac{B}{T(K) - C} \quad (1)$$

where  $A$ ,  $B$  and  $C$  are adjustable parameters, including the pre-exponential factor, pseudo-activation energy, and the VFT-temperature, respectively. On the basis of theoretical and numerical arguments (Myuller, 1955; Eyring et al., 1982; Angell, 1985; Russell et al., 2002, 2003) we assume  $A$  to be an unknown constant. This implies that the compositional controls on viscosity reside only in  $B$  and  $C$ .

#### 3.1. The constant $A$ concept

The parameter  $A$  is the value of  $\log \eta$  (Pa s) at infinite temperature and, thus, represents the high temperature limit to silicate melt viscosity ( $\log \eta_\infty$ ). The assumption that  $A$  is constant for all melts (i.e., independent of composition) implies that all melts converge to a single, common value of viscosity at high-T. The expectation is that at super-liquidus temperatures, all silicate melts will become highly dissociated liquids regardless of their lower temperature structure and converge to lower limiting value of viscosity. The “constant  $A$  concept” is supported by observations on many low-T glass-forming systems including polymer melts (e.g., polyisobutane), organic liquids (e.g., Salol and O-terphenyl) and even liquid elements (e.g., molten Se) (Angell, 1991; Scopigno et al., 2003). In these systems, experiments can be run at temperatures that are well above the corresponding glass transition temperatures (e.g.,  $T_g/T \rightarrow 0$ ) and, thus, can directly explore the high-T properties of melts. These experiments have shown that, at temperatures well above  $T_g$ , both strong and fragile melts commonly converge to a common viscosity (e.g.,  $\eta_{T \rightarrow \infty} \sim 10^{-5}$  Pa s; e.g., Eyring et al., 1982; Angell, 1991, 1995; Russell et al., 2003; Scopigno et al., 2003).

The concept of a high-T limit to silicate melt viscosity (e.g., constant  $A$ ) is also supported by considering the time scales of relaxation processes in melts (Eyring et al., 1982; Angell, 1991, 1995; Richet and Bottinga, 1995; Russell et al., 2003; Scopigno et al., 2003 and reference therein). The Maxwell relationship ( $\tau = \eta_0/G_\infty$ ) can be used to constrain the lower limits to melt viscosity ( $\eta_0$ ). The bulk shear modulus ( $G_\infty$ ) of the melt at infinite frequency can be assigned an average value of  $\sim 10^{10}$  Pa (Dingwell and Webb, 1989; Toplis, 1998). The relaxation time scale ( $\tau$ ) of the melt is dictated by the quasilattice vibration period ( $\sim 10^{-14}$  s) which represents the time between successive assaults on the energy barriers to melt rearrangement (e.g., Angell, 1991; Toplis, 1998). Thus, the lower limiting value to viscosity ( $\eta_0$ ) should approximate  $10^{-4}$  Pa s. Allowing for some variation in these physical constants, would still restrict  $A$  to  $\pm 1$  logunits and establish the high-T viscosity limits for melts at between  $10^{-3.5} - 10^{-5.5}$  Pa s (e.g., Angell, 1991; Toplis, 1998).

#### 3.2. Compositional dependencies

Compositional effects are ascribed to the parameters  $B$  and  $C$  by assuming that both parameters can be expressed as a linear ensemble of combinations of oxide components and a subordinate number of multiplicative oxide cross-terms:

$$B = \sum_{i=1}^7 [b_i M_i] + \sum_{j=1}^3 [b_{ij} (M_{1ij} \cdot M_{2ij})] \quad (2)$$

$$C = \sum_{i=1}^6 [c_i N_i] + [c_{11} (N_{111} \cdot N_{211})] \quad (3)$$

where  $M$ s and  $N$ s refer to the combinations of mol% oxides reported in Table 1 for  $B$  and  $C$ , respectively. Two terms involve logarithms of the volatile contents. The 17 unknown coefficients ( $b_i$ ,  $b_{ij}$ ,  $c_i$ ,  $c_{11}$ ) defined in Eqs. (2) and (3) are suffice to compute the values of  $B$  and  $C$  for any individual melt composition.

#### 3.3. Model optimization

The chemical model comprises 18 adjustable parameters or model coefficients (Table 1), including: i)  $A$ , ii) 10 coefficients ( $b_i$ ,  $b_{ij}$ ) to capture

**Table 1**

Coefficients for calculation of VFT parameters  $B$  and  $C$  [ $A = -4.55 (\pm 0.21)^a$ ] from melt compositions expressed as mol% oxides

Oxides	Values	Oxides	Values
$b_1$ SiO <sub>2</sub> +TiO <sub>2</sub>	159.6 (7)	$c_1$ SiO <sub>2</sub>	2.75 (0.4)
$b_2$ Al <sub>2</sub> O <sub>3</sub>	-173.3 (22)	$c_2$ TA <sup>c</sup>	15.7 (1.6)
$b_3$ FeO(T)+MnO+P <sub>2</sub> O <sub>5</sub>	72.1 (14)	$c_3$ FM <sup>d</sup>	8.3 (0.5)
$b_4$ MgO	75.7 (13)	$c_4$ CaO	10.2 (0.7)
$b_5$ CaO	-39.0 (9)	$c_5$ NK <sup>e</sup>	-12.3 (1.3)
$b_6$ Na <sub>2</sub> O+V <sup>b</sup>	-84.1 (13)	$c_6$ ln(1+V)	-99.5 (4)
$b_7$ V+ln(1+H <sub>2</sub> O)	141.5 (19)	$c_{11}$ (Al <sub>2</sub> O <sub>3</sub> +FM+CaO	0.30 (0.04)
$b_{11}$ (SiO <sub>2</sub> +TiO <sub>2</sub> )*(FM)	-2.43 (0.3)	-P <sub>2</sub> O <sub>5</sub> )*(NK+V)	
$b_{12}$ (SiO <sub>2</sub> +TA	-0.91 (0.3)		
+P <sub>2</sub> O <sub>5</sub> )*(NK+H <sub>2</sub> O)			
$b_{13}$ (Al <sub>2</sub> O <sub>3</sub> )*(NK)	17.6 (1.8)		

<sup>a</sup> Numbers in brackets indicate 95% confidence limits on values of model coefficients.

<sup>b</sup> Sum of H<sub>2</sub>O+F<sub>2</sub>O<sub>-1</sub>.

<sup>c</sup> Sum of TiO<sub>2</sub>+Al<sub>2</sub>O<sub>3</sub>.

<sup>d</sup> Sum of FeO(T)+MnO+MgO.

<sup>e</sup> Sum of Na<sub>2</sub>O+K<sub>2</sub>O.

the compositional controls on  $B$ , and iii) 7 coefficients ( $c_i$ ,  $c_{11}$ ) for  $C$ . We obtained the optimal solution by minimization of the function:

$$X^2 = \sum_{i=1}^n \left[ \left( \log \eta_i - A - \frac{B(x_i)}{(T_i - C(x_i))} \right)^2 / \sigma_i^2 \right] \quad (4)$$

where the summation is over the entire  $n$  experiments and each data array includes observed values of  $\log \eta_i$ ,  $T_i$ , the melt composition ( $x_i$ ) and the experimental uncertainty on  $\log \eta_i$  (i.e.,  $\sigma_i$ ). The optimization involves simultaneous solution of this system of non-linear equations and the methods we used are discussed more fully in Russell et al. (2002) and Russell and Giordano (2005).

The optimal values for the 18 model parameters and their corresponding confidence limits are reported in Table 1; a demonstration calculation is provided for in Table 2. In our model,  $A$  is one of the parameters we solve for and the optimization returns an independent and robust estimate for this high-T limit to viscosity. The optimal value ( $A = -4.55 \pm 0.21$ ;  $\eta_\infty \sim 10^{-4.6}$  Pa s; Table 1) accords well with values ( $\sim 10^5$  Pa s) postulated for low-T glass-forming systems (Bottinga and Weill, 1972) and predicted by theory (Myuller, 1955; Eyring et al., 1982). We have also performed an additional set of numerical experiments to further test the concept that all silicate melts, regardless of composition, converge to a single value at high temperature (Vogel, 1921; Richet and Bottinga, 1995; Russell et al., 2002; Giordano and Russell, 2007). Our experiments involved running the optimization code separately on the datasets for volatile-free ( $N=932$ ) and volatile-rich ( $N=842$ ) melts which returned values for  $A$  of  $-4.36 \pm 0.3$  and  $-4.11 \pm 0.45$ , respectively. The values of  $A$  for partitioned datasets are clearly within error of the value ( $-4.55 \pm 0.21$ ) obtained for the larger optimization problem. We take this as a strong empirical endorsement of the “constant  $A$  concept”.

**Table 2**

Sample calculation of viscosity (Pa s) using model coefficients (Table 1)

Sample <sup>a</sup>	wt.%	wt.% <sub>N</sub>	mol%	B-terms	Values	C-terms	Values
SiO <sub>2</sub>	62.40	61.23	62.38	$b_1$	10018.8	$c_1$	171.5
TiO <sub>2</sub>	0.55	0.54	0.41	$b_2$	-2043.2	$c_2$	191.8
Al <sub>2</sub> O <sub>3</sub>	20.01	19.63	11.79	$b_3$	6.69	$c_3$	40.27
FeO(T)	0.03	0.03	0.03	$b_4$	363.2	$c_4$	99.2
MnO	0.02	0.02	0.02	$b_5$	-379.1	$c_5$	-49.21
MgO	3.22	3.16	4.80	$b_6$	-858.7	$c_6$	-204.5
CaO	9.08	8.91	9.73	$b_7$	1253.4	$c_{11}$	85.3
Na <sub>2</sub> O	3.52	3.45	3.41	$b_{11}$	-738.7		
K <sub>2</sub> O	0.93	0.91	0.59	$b_{12}$	-733.8	$A$ (constant) <sup>b</sup>	-4.55
P <sub>2</sub> O <sub>5</sub>	0.12	0.12	0.05	$b_{13}$	831.6	$B$ (computed) <sup>b</sup>	7720
H <sub>2</sub> O	2.00	2.00	6.80			$C$ (computed) <sup>b</sup>	334

<sup>a</sup> Iron-free andesite melt with 2.00 wt.% H<sub>2</sub>O.

<sup>b</sup>  $\log \eta = A + B/(T(K) - C)$ ; predicted value for this melt at 1273 K is 3.67 Pa s.

An equally valid interpretation, reflecting a numerical modelling perspective, is that, even the highest temperature measurements of melt viscosity, only weakly constrain the value of  $A$ . Thus, one of the strengths of a large scale optimization, such as this, is that the optimal  $A$  must satisfy all of the experimental observations. The consequence is that, as long as the model assumptions are consistent with the data, increasing the number of data in the optimization problem will produce tighter confidence limits on the model parameters. The fact that confidence limits on  $A$  are tightest for the complete dataset provides another level of verification for this model assumption.

Some of the compositional coefficients (i.e.,  $b_{11}$ ,  $b_{12}$ ,  $c_{11}$ ) are small relative to the other coefficients. However, our analysis shows all values to be significant at the 95% confidence level and they cannot be dropped without reducing the quality of the fit (Table 1). Conversely, the total number (17) of compositional coefficients (Eqs. (2) and (3); Table 1) results, in part, from a sequence of earlier optimizations that included additional compositional terms. Higher order models were considered to be overfit and rejected unless they returned a significantly better fit to the original data and all adjustable parameters were shown to be significantly different from zero.

#### 4. Model assessment and comparison

##### 4.1. Model quality

There is excellent agreement between values of viscosity obtained by experiment and those predicted by the model (Fig. 3). The model has a root-mean-square-error (RMSE) of 0.40 log units and anhydrous and hydrous melts have an average misfit ( $|\text{observed} - \text{predicted}|$ ) of  $\pm 0.25$  and  $\pm 0.35$  logunits, respectively. The data plotted in Fig. 3 show that the largest residuals derive from the low-T data where viscosity values

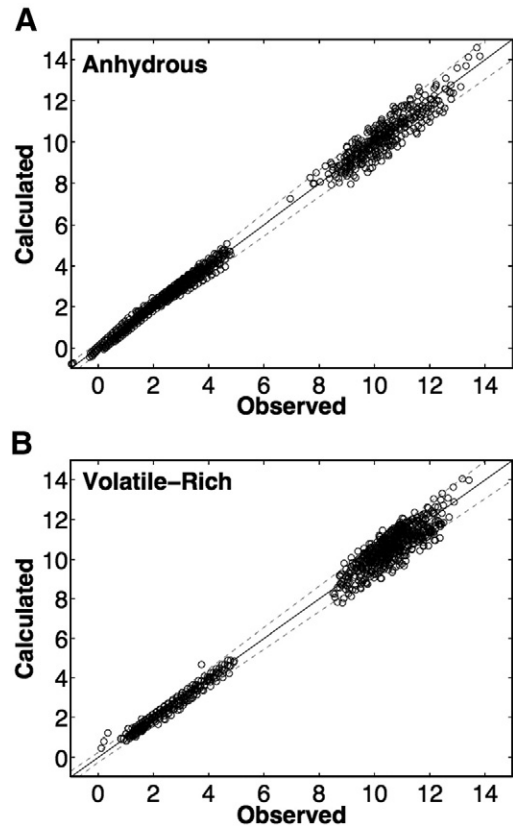


**Fig. 3.** Results of VFT-based model for compositional dependence of silicate melt viscosity. Observed values of viscosity are compared against model values for (A) anhydrous ( $N=932$  experiments) and (B) volatile-rich ( $N=842$  experiments) melts. Dashed lines indicate  $\pm 5\%$  uncertainty on measured values of  $\log \eta$ .

exceed  $10^8$  Pa s (Table 3; Fig. 3A, B). Over this range of viscosity, the absolute values of residuals on volatile-rich melts are slightly larger than those on the corresponding volatile-free melts. However, the accuracy of the model at conditions relevant to volcanic processes is usually within 5% relative error (Fig. 3).

#### 4.2. Model parameters $B$ and $C$

The values of  $B$  and  $C$  calculated from melt compositions using our chemical model (Fig. 4) vary from 4450 to 12,000 J mol<sup>-1</sup>, and -125 to 668 K, respectively. Melts enriched in H<sub>2</sub>O and F show roughly the same range of values for  $B$  (4600 to 12,000 J mol<sup>-1</sup>) compared to anhydrous melts (4450 to 11,950 J mol<sup>-1</sup>) but model values of  $C$  decrease substantially with increased volatile content (Fig. 4; open symbols). The predicted values of  $C$  are substantially lower (-125 to 550 K) for volatile-rich melts than predicted for anhydrous melts (190 to 668 K). Values of  $C$  represent the temperature where the viscosity becomes singular and is related to the Kauzmann temperature, where the entropy difference between solid and liquid is zero. In principle, the values of  $C$  should always be greater than 0 K (cf. Fig. 4).

Values of  $B$  and  $C$  for the 58 anhydrous melts (solid circles; Fig. 4) show a strongly negative linear relationship. The two largest outliers to this general trend are compositions SFB60 (wt.% SiO<sub>2</sub>=74.8) and SFB40 (wt.% SiO<sub>2</sub>=58.9). These outliers derive from the literature (Bouhifd et al., 2004; Appendix B), rather than from our own viscosity measurements, and we cannot comment further on their validity. The predicted values of  $B$  and  $C$  for volatile-enriched melts (grey circles; Fig. 4) show a dramatic departure from the linear pattern established by anhydrous melts. Values of  $B$  for anhydrous melts decrease with increasing proportions of network-modifier cations (i.e. Na, K, Ca, Mg) (Fig. 4). Increasing volatile content causes only a slight decrease in  $B$  (Fig. 4). The values of  $C$  are highest for melts having the highest contents of network-modifiers. In contrast to  $B$ , the  $C$  parameter is strongly dependent on volatile content. Relative to the anhydrous compositions, values of  $C$  decrease strongly with increased volatile contents (Fig. 4). This pattern suggests that, although water and fluorine are normally considered network modifiers, they play a somewhat different role in the structure of silicate melts relative to other network-modifying cations (see discussion below).

#### 4.3. Model comparisons

There are presently a number of models for predicting viscosity of melts as a function of temperature and composition (Shaw, 1972; Bottinga and Weill, 1972; Persikov, 1991; Giordano and Dingwell,

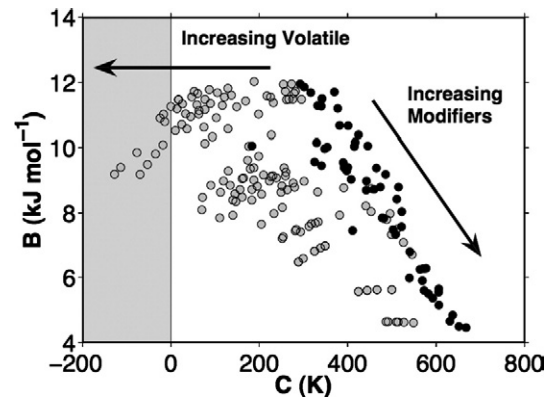


**Fig. 4.** Variations in values of parameters  $B$  (kJ per mole) and  $C$  (K) predicted for volatile-free (solid) and volatile-rich melts by our model for melt viscosity. Predicted values of  $B$  and  $C$  vary from 4400 to 12,000 J mol<sup>-1</sup> and from -120 to 670 K, respectively. Relative to dry melts, melts enriched in H<sub>2</sub>O and F show the same range of  $B$  values but lower values of  $C$  (see text), to 12,000 J mol<sup>-1</sup> and from -120 to 670 K, respectively. Relative to dry melts, melts enriched in H<sub>2</sub>O and F show the same range of  $B$  values but lower values of  $C$  (see text).

2003; Giordano et al., 2006; Hui and Zhang, 2007; Avramov, 2007). Below we compare our model to two of these; the most commonly used Arrhenian model of Shaw (1972) and the most recent non-Arrhenian model of Hui and Zhang (2007). Both of these models are designed for natural hydrous melts. For comparative purposes we have dropped all fluorine-bearing melts from our database as neither of these previous models is calibrated for fluorine.

##### 4.3.1. The Shaw model

The model of Shaw (1972) has an Arrhenian basis of the form  $\log \eta = \log \eta_{\infty} + E_a/T(K)$ , where both  $\log \eta_{\infty}$  and  $E_a$  (i.e., the activation energy) have compositional dependence, and it is calibrated with ~130 experiments spanning a wide range of temperatures (~600 to 1700 °C) and viscosities (~10<sup>-0.2</sup> to 10<sup>12</sup> Pa s). The compositional dependence is embedded in the term the author refers to as a *characteristic slope* ( $s$ ) and which is calculated from melt compositions using a total of 5 model parameters.

We have used the SH model to predict the viscosity of melts in our database (Table 3; Fig. 5). We fully expect it to fail because it has a strictly Arrhenian temperature dependence and cannot possibly cope with the slight to pronounced non-Arrhenian behaviour shown by most natural melts. Table 3 is a statistical analysis of how well the SH model reproduces our experimental database after removing the F-bearing melts. The model is applied to the anhydrous, hydrous and combined (anhydrous+hydrous) datasets. As expected, the SH model reproduces the data poorly (cf. values of  $\chi^2$ ) and RMSE values are 5–8 times higher than obtained by our model (GRD). The SH model does a good job of reproducing melt viscosity at high temperatures (Fig. 5A, B). This reflects the fact that most silicate melts show near-Arrhenian behaviour at liquidus conditions. However, it is also a testament to the robustness of this parameterization (Shaw, 1972). At lower temperatures the SH model systematically misses the anhydrous dataset by always underestimating melt viscosity (Fig. 5A). This results from the Arrhenian model being linearly extrapolated to lower temperatures coupled to the fact that viscosity curves for all non-Arrhenian silicate melts are concave up (Fig. 2) and steepen with decreasing temperature. Hydrous melts show a similar pattern except that the systematic deviation is not as pronounced and there are some melts for which the SH model overestimates melt viscosity (Fig. 5B). Hydrous melts tend to be more Arrhenian-like than their anhydrous counterparts (see below) and, thus, the SH model can be applied to hydrous melts over larger temperature intervals.

Using the Shaw (SH) model, we have also calculated values of  $\log \eta_{\infty}$  for all anhydrous and hydrous melts in the viscosity database. This parameter in the SH model represents the high-T limit to melt

**Table 3**  
Statistical comparison of models for predicting silicate melt viscosity

Model <sup>a</sup>	Dataset		Anhydrous	Volatile-rich	Total
GRD	F-free data <sup>b</sup>	$N$	932	590	1508
		$\chi^2$	6549	1775	8325
		RMSE <sup>c</sup>	0.34	0.50	0.41
SH		$\chi^2$	251,356	35,020	286,377
		RMSE	2.53	2.47	2.51
HZ		$\chi^2$	24,096	2300	26,396
		RMSE	0.52	0.54	0.53
HZ	HZ-data	$N$	757	694	1451
		RMSE	0.33	0.28	0.31
GRD	Full dataset	RMSE	0.91	0.71	0.82
GRD		$N$	932	842	1774
GRD		$\chi^2$	6993	2232	9226
		RMSE	0.34	0.46	0.40

<sup>a</sup> GRD: model for viscosity of volatile-rich melts presented here and calibrated on 1774 experiments; HZ: model of Hui and Zhang (2007); SH: model of Shaw (1972).

<sup>b</sup> All data in GRD database excluding F-bearing compositions for comparative purposes.

<sup>c</sup> RMSE is the root mean square error.

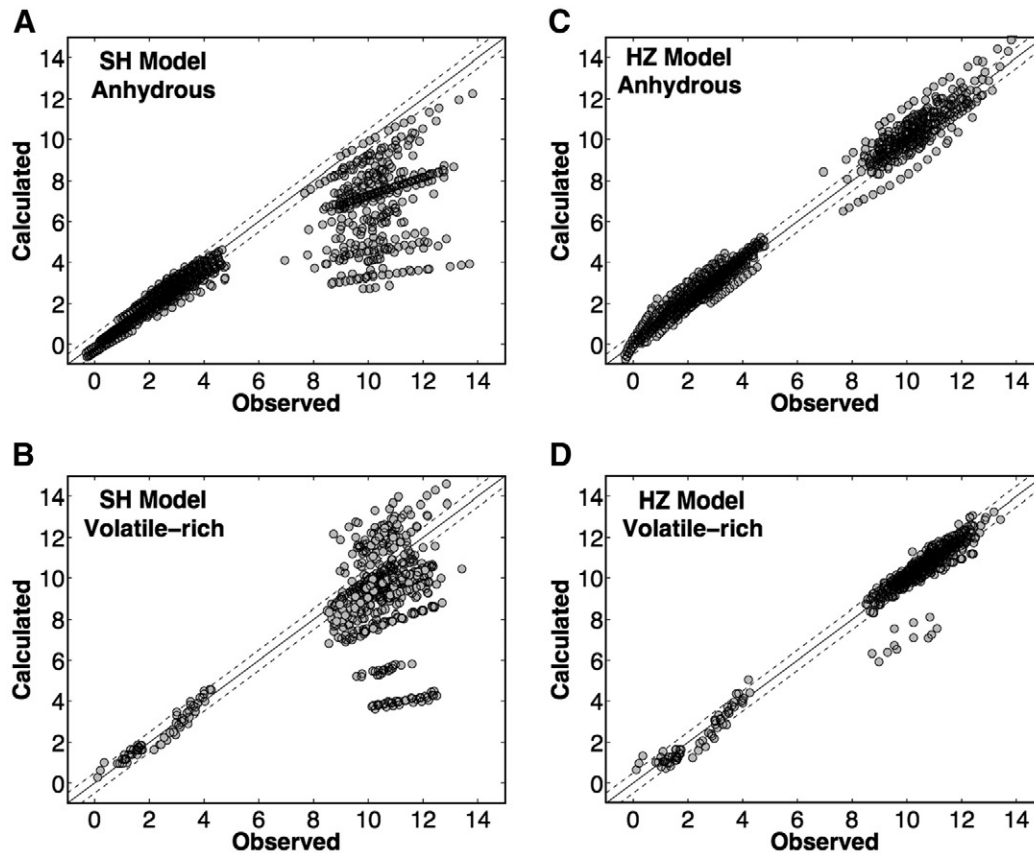


**Fig. 5.** Prediction of melt viscosity using previously published models (Table 3). Observed values of  $\log \eta$  from our database are plotted vs. values calculated with models of: (A, B) Shaw (1972) (SH) and (C, D) Hui and Zhang (2007) (HZ). Datasets are separated into anhydrous (A, C) and hydrous (B, D) suites. Melts from our database containing fluorine were excluded.

viscosity and varies between  $-6$  and  $-4.0$  ( $\eta_{\infty} = 10^{-6}$  to  $10^{-4}$  Pa s; Fig. 6A). Thus, it is implicit to the SH model that all silicate melts converge to a nearly constant viscosity at high temperatures.

#### 4.3.2. The Hui and Zhang model

The Hui and Zhang (2007) model (HZ) for hydrous silicate melts is based on the empirical equation [ $\log \eta = A + B/T(K) + \exp(C + D/T(K))$ ] and is intended to handle the non-Arrhenian temperature dependence of melt viscosity (Hui and Zhang, 2007). The model comprises 37 adjustable parameters, is calibrated against 1451 experimental measurements, and purports to reproduce these data to within 0.61 log units at the 95% confidence level. We performed a similar exercise of using the HZ model to reproduce our database (Fig. 5C, D; Table 3). The HZ model reproduces our database well although the  $\chi^2$  values (residuals weighted to our uncertainties; Eq. (4)) are 2–3 times higher and the RMSE values are 10–50% higher than the values corresponding to our model (cf. Table 3). A plot of observed values vs. HZ model values (Fig. 5C, D) shows that their model reproduces the high-T (near liquidus) viscosity data. As observed for the GRD model (Fig. 3), the largest deviations between observed and model values are for the low-temperature measurements on hydrous melts.

We also compared how well our model (GRD) reproduces the original dataset ( $N=1451$ ) used to calibrate the HZ model (Table 3). The RMSE for our model are  $\sim 2.5$  times higher than achieved by the HZ model which largely reflects the fact that their model uses more than twice the number of model parameters to reproduce their calibration dataset.

The HZ model does not explicitly define the high temperature limits on melt viscosity, however, these limits are implicit and we have explored them using the full range of anhydrous and hydrous melt compositions from the HZ and GRD databases (Fig. 6A). For 58 anhydrous melt

compositions the HZ model predicts values of  $\eta_{\infty}$  that range from  $10^{-9}$  to  $10^{-1.3}$  Pa s and has an average value of  $10^{-1.6}$  Pa s. The hydrous melts ( $> 120$  compositions) are predicted to have high temperature limits on  $\eta_{\infty}$  of  $10^{-9}$  to  $10^{+0.4}$  Pa s and an average of  $10^{-3.2}$  Pa s. This wide range of values for  $A$  (i.e.,  $\log \eta_{\infty}$ ) is a trait of the HZ model. The fact that the model allows for these unphysical limits represents a significant flaw and limits the potential use of the model outside of the range of temperatures and melt compositions used to calibrate the 37 parameter model. Another disadvantage of the HZ model is that the form of their base equation precludes direct connection of the model parameters to intrinsic melt properties such as activation energy, glass transition temperature, and fragility (Shaw, 1972; Dingwell, 1996; Baker, 1996; Dingwell and Hess, 1998; Bourgue and Richet, 2001; Russell et al., 2002; Giordano and Dingwell, 2003; Zimova and Webb, 2006; Giordano et al., 2006; Hui and Zhang, 2007).

## 5. Model consequences

The quality of our model is demonstrated, in part, by how well it reproduces measured values of melt viscosity (Fig. 3). However, higher-level models have the power to extrapolate and have logical consequences that can serve as testable predictions (Greenwood, 1989). The model we have presented here can be tested against the expected behaviour of other transport properties with respect to composition (Figs. 7 and 8).

### 5.1. Compositional controls on $B$ and $C$

In our model, all compositional controls on viscosity reside in the parameters  $B$  and  $C$ . The relationships between these parameters and melt composition, represented by NBO/T and  $H_2O$  content, are

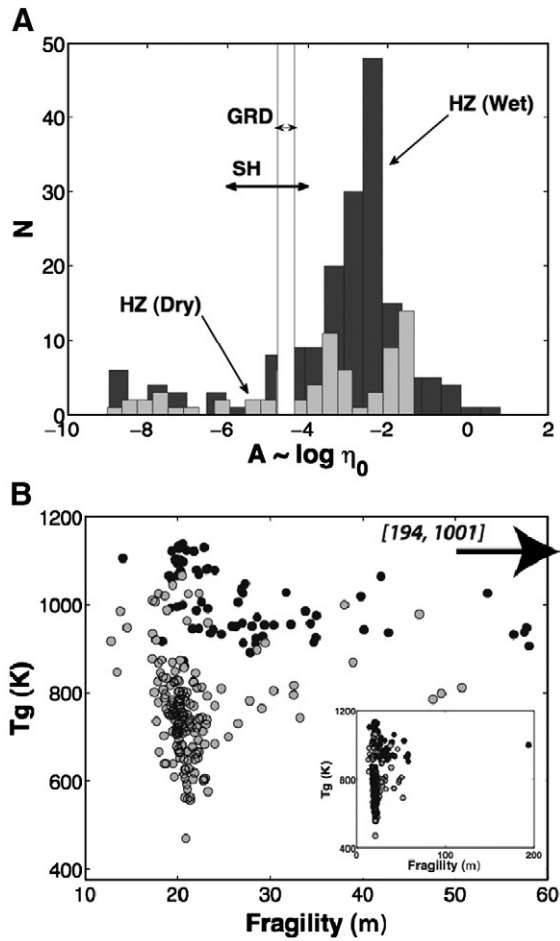


**Fig. 6.** Properties implicit in other melt viscosity models. (A) Values of  $A$  representing the high-T limits to silicate melt viscosity (i.e.  $\log \eta_\infty$ ) implicit in the SH model (Shaw, 1972), the HZ model (Hui and Zhang, 2007) and our model (GRD). The GRD model solves for a single, high-T limit for silicate melt viscosity independent of composition ( $-4.6 \pm 0.2$ ). The SH model predicts values of  $A$  between  $-4$  and  $-6$  for the entire range of anhydrous and hydrous melts in the calibration database. The HZ model ascribes a compositional dependence to the high-T limit on viscosity and, for the same dataset, the HZ model predicts 10 orders of magnitude variations in  $A$ . (B) Values of  $T_g$  (K). The SH model predicts values of  $A$  between  $-4$  and  $-6$  for the entire range of anhydrous and hydrous melts in the calibration database. The HZ model ascribes a compositional dependence to the high-T limit on viscosity and, for the same dataset, the HZ model predicts 10 orders of magnitude variations in  $A$ . (B) Values of  $T_g$  (K). The SH model predicts values of  $A$  between  $-4$  and  $-6$  for the entire range of anhydrous and hydrous melts in the calibration database. The HZ model ascribes a compositional dependence to the high-T limit on viscosity and, for the same dataset, the HZ model predicts 10 orders of magnitude variations in  $A$ . (B) Values of  $T_g$  (K) and fragility ( $m$ ) predicted by the HZ model. Inset shows values for all melt compositions including one aberrant point which plots at  $[m=194; T_g=1001]$  (see text for discussion).

illustrated in Fig. 7. Model values of  $B$  for dry melts decrease regularly with increasing NBO/T (Fig. 7A) which is an expected pattern; increasingly depolymerized melts should show a concomitant decrease in melt activation energies (proportional to  $B$ ) (Richet and Bottinga, 1995; Mysen, 1988). Volatile-free and volatile-rich melts have overlapping ranges of  $B$  values and, both, show pronounced decreases in  $B$  with increasing NBO/T. Values of  $C$  show a different pattern against NBO/T (Fig. 8B). The values of  $C$  are highest for melts having the highest contents of network-modifiers and, thus, highest values of NBO/T. Anhydrous melts show a marked and regular increase in  $C$  ( $> 300$  K) with increasing NBO/T ( $> 1.5$ ) implying that depolymerized dry melts have higher VFT temperatures (e.g., C Richet and Bottinga, 1995). Increasing volatile content causes a slight increase in NBO/T relative to the marked decrease in values of  $C$  (Figs. 4 and 7B).

The effects of the volatiles on the  $B$  and  $C$  parameters are illustrated more fully in Fig. 7C and D by applying our viscosity model to a variety of melt compositions. Each curve represents a

single anhydrous melt composition to which  $H_2O$  is added; values of  $B$  and  $C$  are computed for each of these derived melt compositions. The open symbols denote compositions for which there are experimental data. Increasing volatile content causes a slight decrease in  $B$  (Figs. 4 and 7C). The decrease in values of  $B$  with increasing water content (e.g., the slope in Fig. 7C) is most pronounced for anhydrous melts that have the highest values of  $B$ . Anhydrous melts with low values of  $B$  can maintain near constant  $B$ -values with increasing water contents. The  $C$  parameter is even more strongly dependent on volatile content. Relative to the anhydrous compositions, values of  $C$  decrease strongly with increased volatile contents (Figs. 4 and 7D). In summary, water has a different influence on the values of  $B$  and  $C$  relative to other network modifying cations. This suggests that it plays a somewhat different role on the values of  $B$  and  $C$  suggesting that water may play a somewhat different role in the structure of silicate melts relative to other network-modifying cations (Dingwell, 1991).

## 5.2. Transport properties

We have used the viscosity model to investigate the compositional controls on other derivative transport properties of glass-forming materials, such as the glass transition temperature ( $T_g$ ) and the fragility  $m$  of silicate melts (Fig. 8).  $T_g$  is the temperature separating the liquid (relaxed) from the glassy (unrelaxed) state and is taken, here, as the temperature corresponding to a viscosity of  $10^{12}$  Pa s. This value of  $T_g$  is calculated from Eq. (1) as  $C+B/(12-A)$  (Angell, 1985; Dingwell et al., 1993). This value of viscosity corresponds to a relaxation timescale for macroscopic melt properties of about 15 min and to cooling rates of  $\sim 10$  K/min.

Melt fragility is a measure of the sensitivity of liquid structure and flow properties to changes in temperature and it distinguishes two extreme behaviours of glass-forming liquids: *strong vs. fragile* (Angell, 1985). “Strong” liquids show near-Arrhenian temperature dependence and show a firm resistance to structural change, even over large temperature variations. Conversely, “fragile” liquids show non-Arrhenian temperature dependence indicating that thermal perturbations are accommodated by continuous changes in melt structure. The “steepness index” ( $m$ ), as defined by Plazek and Ngai (1991), is a common measure of melt fragility used to track departures from Arrhenian behaviour and to distinguish strong and fragile melts. Essentially, it is the slope of the viscosity trace taken at  $T_g$  and can be calculated as:

$$m = \left. \frac{d(\log_{10} \eta)}{d(T_g/T)} \right|_{T=T_g} = \frac{B}{T_g(1-C/T_g)^2} \quad (5)$$

where  $B$ ,  $C$  and  $T_g$  are specific properties of the individual melts (e.g., rhyolite vs. basalt). Low values of  $m$  correspond to strong (Arrhenian-like) melts and higher values of  $m$  indicate increasing fragility (non-Arrhenian). It is important to note that the parameter  $m$  gives no new information not already included in  $A$ ,  $B$  and  $C$  (Eq. (5)) because  $T_g$  is, itself, a function of the VFT parameters.

Fig. 8A shows the calculated values of  $T_g$  and  $m$  for all melts in our database. Anhydrous melts show a wide range in fragility ( $m$ ) indicating that the database comprises both strong and moderately fragile melts. Values of  $T_g$  for anhydrous melts vary slightly but are not strongly correlated with fragility. The transport properties  $T_g$  and  $m$  are strongly affected by volatile contents (Fig. 8). The main effect of increased volatile content is to depress values of  $T_g$  (Fig. 8A, B) and  $m$  (Fig. 8A, C). Model values of  $T_g$  decrease precipitously with increasing  $H_2O$  content (Fig. 8B) and accord well with experimental studies (Hess and Dingwell, 1996; Giordano et al., 2004a,b). The largest decrease in  $T_g$  (150–225 K) is predicted to occur within the first 5 mol% of  $H_2O$ . Anhydrous melts with  $T_g$  values of 900–1066 K have predicted  $T_g$  values of 500–700 K at 20 mol%  $H_2O$  (Fig. 8B).

Dissolved volatiles also cause a reduction in fragility (Fig. 8A, C). Comparing model values of  $m$  over the entire experimental database

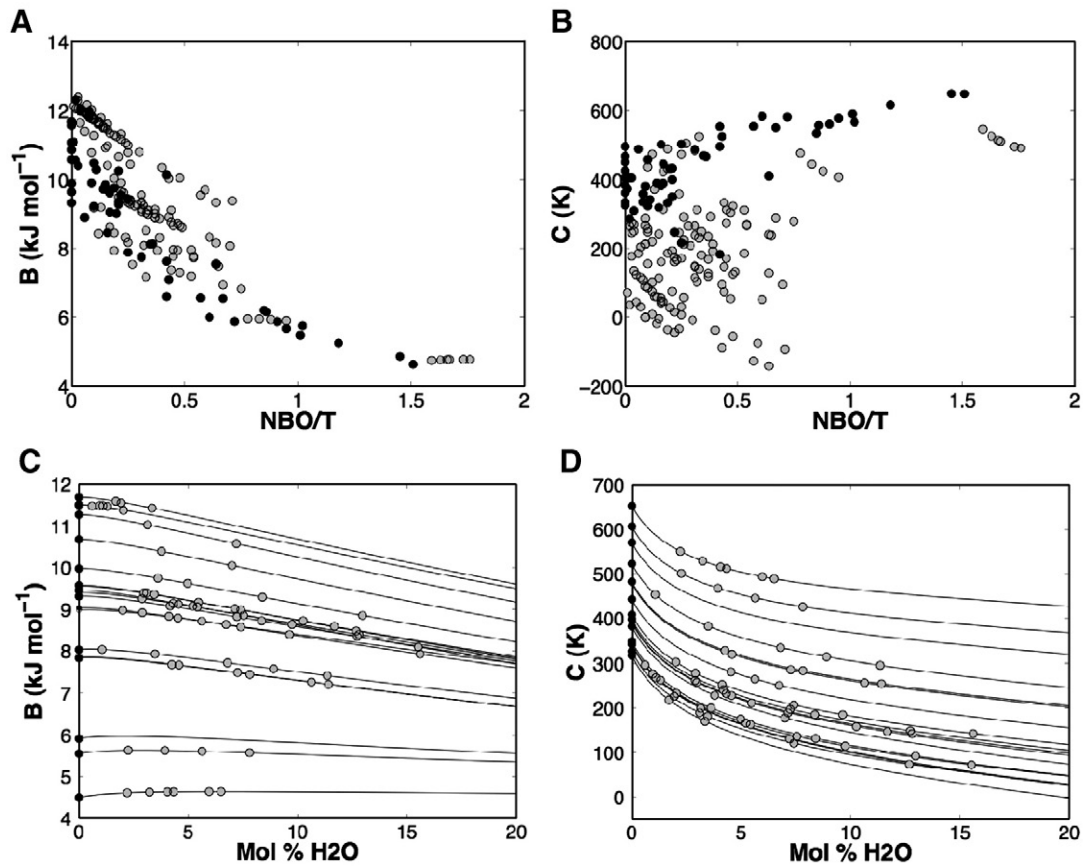


**Fig. 7.** Variations in model values of  $B$  and  $C$  relative to composition as represented by the ratio of non-bridging oxygens to tetrahedrally-coordinated cations (NBO/T) and H<sub>2</sub>O content (mol%). (A, B) Model values of  $B$  (kJ mol<sup>-1</sup>) and  $C$  (K) are plotted against NBO/T for anhydrous (solid symbols) and volatile-enriched (grey symbols) melts. (C, D) Calculated curves showing changes in parameters  $B$  and  $C$  for a range of melt compositions as they become increasingly hydrated (see text for discussion).

shows a total variation of 20–58 for anhydrous melts vs. 12–49 for volatile-rich equivalents (Fig. 8A). The implication is that volatiles cause melts that are moderately depolymerized to become less *fragile* (e.g., *stronger* as defined by the  $m$  parameter). The corollary is that dry melts that show non-Arrhenian behaviour tend to become more Arrhenian with increasing volatile content. The effect of volatiles on melt fragility is greatest for the most fragile melts (highest values of  $m$ ) and least for strong melts (Fig. 8C). This trend is, at first glance, somewhat counter-intuitive because the normal effect of adding network-modifier cations (e.g., increasing NBO/T) is to increase fragility. The potential of water to cause depolymerization of silicate melts and, thus, a reduction in NBO/T has, however, been hotly debated (Kohn, 2000).

In summary, the dominant effect of dissolved volatiles is to cause a dramatic decrease in  $T_g$  and a subordinate decrease in  $m$ . For example, at 20 mol% H<sub>2</sub>O the relative decreases in  $m$  and  $T_g$  can be up to 30% and 50%, respectively (Fig. 8B, C). The temperature dependence of viscosity for volatile rich melts appears to be a special case whose detailed nature may in fact be related to temperature-dependent speciation reactions involving the volatile components (Kohn, 2000).

### 5.3. Comparison of model transport properties

One means of assessing the quality of the multicomponent model is to compare its predicted properties against the values that would result from fitting the VFT function to individual datasets for each melt composition. This presumes that fitting the individual datasets provides a closer approximation to the true values of  $T_g$  and  $m$ . Values of  $T_g$  (791–1077 K) and  $m$  (21–58) calculated for 58 anhydrous melts

using our viscosity model (Fig. 7) are in strong agreement with the values obtained by fitting the datasets separately (789–1154 K and 24–65, respectively). In fact, values agree to within 5–10% relative error although values of fragility from the chemical model are systematically lower. This correspondence indicates that the multicomponent model preserves the fundamental properties of most silicate melts. Furthermore, all model values of  $T_g$  (Fig. 8A) are positive, thus physically reasonable, despite the most volatile-enriched melts having negative values of  $C$  (Fig. 4).

We have computed corresponding values of  $T_g$  and  $m$  for the same melt compositions as shown in Fig. 8A using the HZ model (Fig. 6B). The HZ produces a range of values for  $T_g$  and  $m$  that is similar to the range predicted by our model except for a single melt composition (Inset Fig. 6B:  $T_g \sim 1000$  K and  $m \sim 190$  for peridotite). Compared to our model values (Fig. 8A), the  $T_g:m$  values predicted by the HZ model (Fig. 6B) are more scattered and make a much less coherent pattern. Anhydrous melts define a diffuse horizontal band at a  $T_g$  of  $\sim 950$ – $1100$  K and the hydrous melts define a vertical band at a fragility of  $\sim 20$ .

## 6. Applications

Our multicomponent chemical model provides a means to predict the viscosity of volatile-enriched melts. It does so over the full range of compositions found in naturally-occurring silicate melts. A feature that sets this model apart from all others is that it allows for accurate, *continuous* prediction of melt properties as a function of temperature and melt composition. The effects of pressure on the silicate melt viscosity are not accounted for in this model. Natural systems feature constantly

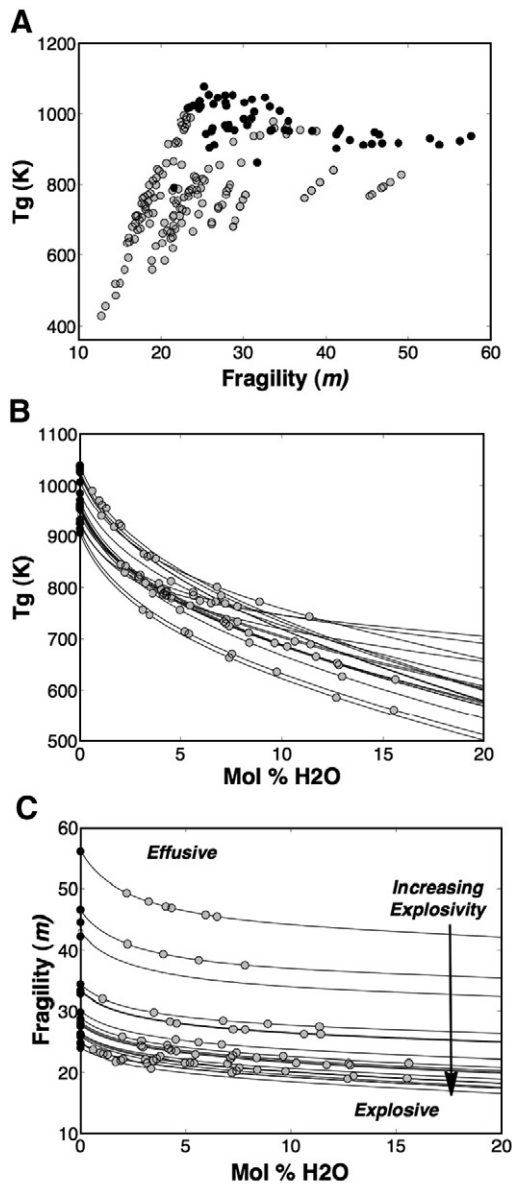


**Fig. 8.** Additional properties of silicate melts predicted by melt viscosity model. (A) Computed values of  $T_g$  (K) vs. melt fragility ( $m$ ) for dry (solid symbols) and volatile-rich (open symbols) melts. (B) Model curves showing depression of  $T_g$  (K) with increasing H<sub>2</sub>O content (mol%) for diverse melt compositions including: basanite, trachybasalt, tephrite, andesite, phonolite, and metaluminous to peralkaline felsic magmas. (C) Model curves for fragility ( $m$ ) vs. H<sub>2</sub>O content (mol%) for same melts as shown in (B). Explosive volcanic behaviour is favoured by melts having low fragility (e.g., strong) at high volatile contents.

changing T-X melt conditions and, in many instances, small changes generate strong non-linear variations in melt viscosity. Our model uses a single computational strategy independent of whether melts are hydrous or anhydrous and strong or fragile and, thus, is mathematically continuous in the T-X space. This property ensures that dramatic shifts in predicted viscosity reflect the changes in melt composition or T as opposed to numerical artefacts (Shaw, 1972; Bottinga and Weill, 1972). This new model should, therefore, lead to more realistic computational models of volcanic processes (Papale, 1999; Sparks, 2004) by predicting changes in melt rheology more accurately. Below we demonstrate the utility and robustness of this model with two sets of model calculations (Table 4; Streck and Grunder, 1995; Whittington et al., 2001; Giordano and Dingwell, 2003; Goto et al., 2005).

### 6.1. Binary mixing of felsic and mafic melts

Models allow extrapolation from known points to domains where there are few or no observations. In Fig. 9 we have used the model to explore the potential consequences of mixing between basanite and rhyolite melts in the absence of crystallization or vesiculation. These calculations have two purposes. Firstly, they demonstrate some of the complex non-intuitive rheological consequences of mixing disparate melts. Secondly, they represent a series of logical consequences that could be pursued experimentally to test our model.

The model viscosity curves reproduce the measurements made on the two end-members (Fig. 9A) and show the viscosities of melts derived from mixing of the end-members in 10% increments. The pattern is simple in that rhyolite melt and the mixtures of rhyolite-basanite, have higher viscosities than the basanite except at temperatures  $< \sim 700$  °C. Adding rhyolite to basanite causes a relative increase in viscosity under all conditions except below this temperature.

Adding 3 wt.% H<sub>2</sub>O to the rhyolite end-member changes the topology of the diagram considerably (Fig. 9B). The viscosity curves for rhyolite and the binary mixtures are drastically depressed. Furthermore, the cross-over point, where basanite first intersects another viscosity curve, now occurs at  $\sim 1020$  °C. At this temperature and below, the viscosity of basanite melt can be greater than the viscosity of mixed melts. At temperatures below 725 °C, basanite has a higher viscosity than the hydrous rhyolite melt. Essentially the viscosity diagram is divided into two regimes: i) a high temperature ( $> 1020$  °C) domain where adding rhyolite to basanite always causes a relative increase in viscosity, and ii) a lower temperature part ( $< 1020$  °C) where adding rhyolite to basanite causes a reduction in melt viscosity.

Lastly, we have plotted the calculated values of  $T_g$  and fragility ( $m$ ) for the melt mixtures (Fig. 9C). The mixed melt compositions are a linear combination of the end-member melts yet they can produce linear or strongly non-linear variations in transport properties. In this diagram (Fig. 9C), basanite is mixed with rhyolite containing between 0 and 3 wt.% H<sub>2</sub>O. The resulting values of  $T_g$  and fragility are indicated by solid lines with circles to mark 10% increments. In every case, mixing any rhyolite melt into basanite causes a reduction in melt fragility suggesting that the mixtures become increasingly Arrhenian with increasing rhyolite content. Values of  $T_g$  for mixed melts show a different pattern. At high water contents ( $> 2$  wt.%) adding rhyolite to

**Table 4**

Summary of melt compositions used in model calculations and their calculated properties, including VFT parameters glass transition temperature ( $T_g$ ) and fragility (F)

Label <sup>a</sup>	GOTO	GOTO	EIF	RST
Rock type	Rhyolite	Rhyolite	Basanite	Rhyolite
Fig. #	9	9	9	10
SiO <sub>2</sub>	76.38	76.38	41.17	76.29
TiO <sub>2</sub>	0.06	0.06	2.74	0.14
Al <sub>2</sub> O <sub>3</sub>	11.59	11.59	12.10	12.04
FeO(T)	1.03	1.03	10.10	1.37
MnO	0.05	0.05	0.18	0.08
MgO	0.36	0.36	11.24	0.04
CaO	3.25	3.25	15.66	0.30
Na <sub>2</sub> O	2.44	2.44	2.76	3.39
K <sub>2</sub> O	4.66	4.66	3.04	4.89
P <sub>2</sub> O <sub>5</sub>	0.00	0.00	1.02	0.01
H <sub>2</sub> O	0.00	3.00	0.00	2.00
F <sub>2</sub> O <sup>-1</sup>	0.00	0.00	0.00	0
A	-4.55	-4.55	-4.55	-4.55
B	11,495	10,542	4457	11,196
C	342	102	669	93.4
$T_g$ (K)	1037	739	938	770
F	24.7	20.0	57.7	18.8

<sup>a</sup> Sources: Goto et al. (2005); EIF (Giordano and Dingwell, 2003); RST (Streck and Grunder, 1995).

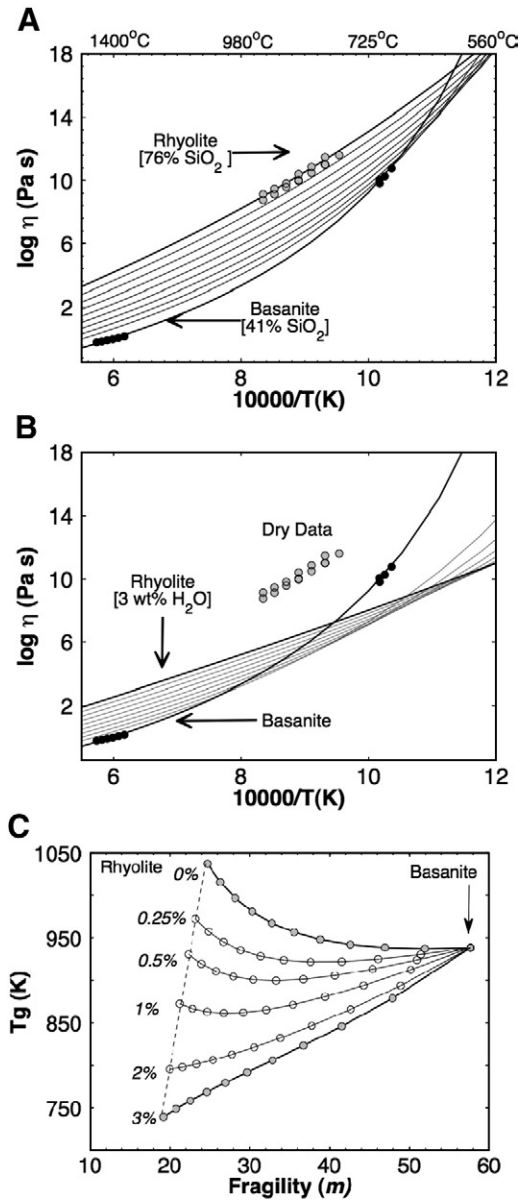


**Fig. 9.** Properties of melts in binary system rhyolite and basanite (Table 4). (A) Comparison of measured values of viscosity (symbols) for rhyolite and basanite melts to temperature-dependent curves for end-member compositions (heavy lines) and 10% mixtures. (B) Parallel model calculations are shown for a hydrous (3 wt.%) rhyolite end-member. (C) Model values of  $T_g$  and fragility ( $m$ ) predicted for rhyolite, basanite and mixtures. Heavy lines denote  $T_g$ - $m$  values for binary mixtures of basanite: anhydrous rhyolite or basanite:rhyolite with 3%  $\text{H}_2\text{O}$ . Dashed line shows  $T_g$ - $m$  values for rhyolite as a function of  $\text{H}_2\text{O}$  content.

anhydrous basanite causes a constant decrease in  $T_g$ . However, mixing of dry rhyolite into basanite melt causes a non-linear increase in  $T_g$ . There is essentially no change in  $T_g$  until >30% rhyolite is added to basanite at which point  $T_g$  rises dramatically. Mixing curves for marginally hydrous (0.25–1%) rhyolite and basanite have minima in  $T_g$  where both end-members have  $T_g$  values higher than the mixtures.

## 6.2. Ascent of degassing magma

Our second calculation is to simulate the ascent of a hydrous melt to demonstrate the potential rheological consequences of a magma degassing during ascent. The melt composition is rhyolitic and taken from the Rattlesnake Tuff (Table 4); for the purposes of modelling it is assumed to

have 2 wt.% dissolved  $\text{H}_2\text{O}$  and have a pre-eruptive temperature of 860 °C (Whittington et al., 2001). Using these starting conditions, we have used MELTS (Ghiorso and Sack, 1995) to simulate the thermodynamic state of the magma as it ascends isothermally and undergoes equilibrium degassing. MELTS modelling predicts the point of volatile saturation for the melt and tracks the decrease in the melt's water content (Fig. 10A) and increasing vol.% of the gas phase (Fig. 10B) as a function of pressure. These variables are used to compute the viscosity of the melt (Fig. 10C) as well as its  $T_g$  and fragility ( $m$ ) (Fig. 10D). As the magma ascends, it begins to degas at ~1100 m depth and the melt phase loses  $\text{H}_2\text{O}$  to the fluid phase; melt viscosity increases 2–3 orders of magnitude (Fig. 10C). We have also modelled the concomitant reduction in magma viscosity ( $\eta_m$ ) due to the increasing volume fraction of bubbles (porosity,  $\phi$ ) using the phenomenological relationship:

$$\log \eta_m = \log \eta_o - \frac{\alpha \cdot \phi}{(1 - \phi)} \quad (6)$$

where  $\eta_o$  is the viscosity of the melt phase calculated at each point. The curves for  $\log \eta_m$  in Fig. 10C were computed using a range of values for  $\alpha$  from the literature (Bagdassarov and Dingwell, 1992; Russell and Quane, 2005). While the viscosity of the melt increases to  $10^9$  Pa s, the effective viscosity of the magma may decrease by 2–3 orders of magnitude. The  $T_g$  and fragility of the degassing melt increase steadily during ascent ( $m$ : 18–22;  $T_g$ : 750–950 K) due to degassing. The implications are that the melt is becoming more non-Arrhenian in its temperature dependence and that the melt's potential for explosive fragmentation is increasing, respectively.

## 7. Conclusions

We have presented a computational model that predicts, within inter-laboratory experimental error, viscosity and other melt properties (i.e.,  $T_g$  and  $m$ ) for most of the T-X space found in naturally-occurring silicate melts. The model accommodates the properties of *fragile* (non-Arrhenian) to *strong* (near-Arrhenian) melts equally well. The model also reproduces the T- $\log \eta$  relationships for melts not used for calibration purposes (see Appendix A) suggesting that the model can be extrapolated past the original database. These attributes make the model useful for predicting the transport properties of melts under conditions (T-X- $X_{\text{H}_2\text{O}}$ ) that do not allow direct experimental measurement (e.g., peridotite, kimberlite, or high-T, volatile-rich melts) (Dingwell et al., 2004).

Despite the strengths of this model, there remains substantial room for improvement. Firstly, our model incorporates the effects of the volatile components  $\text{H}_2\text{O}$  and F, but does not account for other volatiles that may be potentially important under certain conditions including:  $\text{CO}_2$ , sulphur, chlorine. Secondly, we have treated iron as a single species (e.g.,  $\text{FeO}_{\text{Total}}$ ) whereas silicate melts contain both ferric and ferrous iron and their proportions affect melt structure substantially (Mysen, 1988; Dingwell, 1991). At present, there is insufficient experimental data to model the effect of iron redox on melt viscosity. Attempts to do so yield no improvement of fit. Thirdly, we have ignored the effects of pressure on melt viscosity (Avramov, 2007). The pressure dependence of viscosity, although minor compared to the effects of varying temperature and composition, is needed if we are to model melt transport accurately within the deeper crust and mantle. Lastly, our model is strictly empirical, in that, the chemical components we have chosen (Table 1) have no explicit or independent relationship to the structure or speciation of the silicate melt. Ultimately, future models may benefit immensely from the use of a component basis that is, at least in part, a reflection of melt speciation.

## Acknowledgements

A portion of this research was completed when D. Giordano held a post-doctoral fellowship from the Dorothy Killam Trust administered by The University of British Columbia. JKR is supported by the Natural Sciences and Engineering Research Council of Canada. This work was

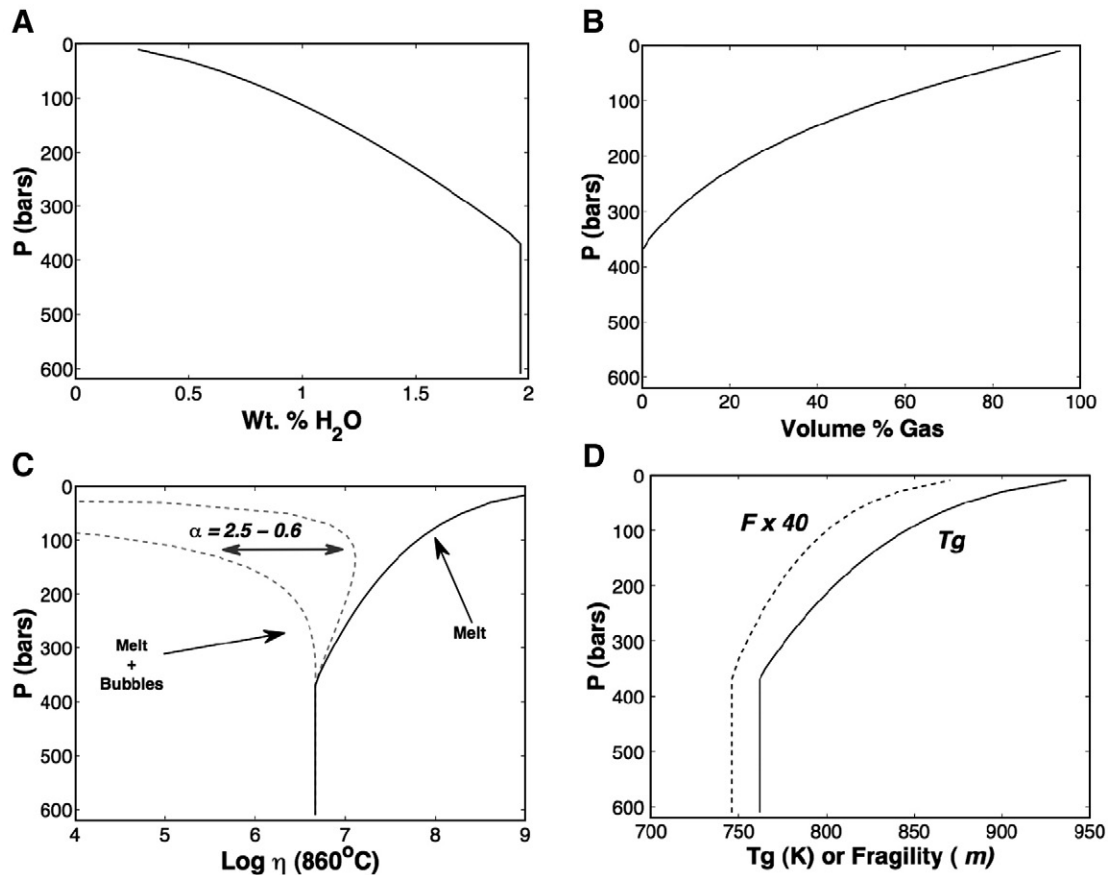


**Fig. 10.** Melt transport properties resulting from ascent and vesiculation of hydrous rhyolite magma. Calculations use melt composition (Table 4) and pre-eruption temperature (860 °C) of Rattlesnake Tuff reported by Streck and Grunder (1995). Model results from MELTS are summarized as: (A) composition (wt.% H<sub>2</sub>O) of ascending and degassing melt and (B) vol.% of the fluid phase plotted against confining pressure. Model assumes an initial H<sub>2</sub>O-content of 2.0 wt.%, isothermal ascent, and equilibrium degassing. Consequences of ascent path for melt transport properties, include: (C) an increase in isothermal melt viscosity due to loss of H<sub>2</sub>O and a potential decrease in magma viscosity due to increasing bubble content (Bagdassarov and Dingwell, 1992; Russell and Quane, 2005), and (D) rapid increase in  $T_g$  (K) and melt fragility with degassing. See text for discussion.

supported by the 2005–2006 INGV-DPC project V3-2/UR17. Experimental viscometry activities of Dingwell's group contributing to the completeness of the data set that was a prerequisite for this model have been supported by the German Science Foundation, The European Commission, the Alexander-von-Humboldt Foundation, the University of Munich, the state of Bavaria and the Gruppo Nazionale di Vulcanologia. The manuscript benefited from critical and thoughtful reviews from Don Baker, Frank Spera and an anonymous referee.

#### Appendix A. Testing the multicomponent model with non-calibration datasets

Our model predicts, within inter-laboratory experimental error, viscosity and other melt properties (i.e.,  $T_g$  and  $m$ ) for most of the T-X space found in naturally-occurring silicate melts. Here we show that the model also reproduces the  $T(K)$ - $\log \eta$  relationships for melts that are not part of the original database used for calibration purposes. We have compiled 257 additional measurements of viscosity [published and unpublished] on diverse melt compositions over a temperature range of 385–1640 °C and a range of viscosity from  $10^{0.7}$  to  $10^{15}$  (cf. Fig. 2). The melt compositions ( $N=179$ ) include rhyolite, phonolite, dacite, shoshonite, tephrit-phonolite and phono-tephrite and have ranges in oxide composition (wt.%) of: SiO<sub>2</sub> (47–79), Al<sub>2</sub>O<sub>3</sub> (11–21), FeO (0–9), MgO (0–5), and total alkalis (3–16). The non-calibration dataset also includes melts enriched in H<sub>2</sub>O ( $N=48$ ; <5 wt.%) and F ( $N=30$ ; <0.5 wt.%).

Fig. A1 shows the comparison between the measured values of  $\log \eta$  and calculated model values. On average, the model reproduces

these data to within experimental tolerance. The highest RMSE is for the anhydrous melts (Fig. A1A). At high temperature (low viscosity) the model reproduces the experimental data to within experimental uncertainties; the low temperature anhydrous data show more scatter. However, the majority of the scatter (and 50% of the residuals) in these data derives from low-temperature measurements on a single rhyolite melt composition. Inspection of the original data (Neuville et al., 1993) shows that, based on replicate measurements of viscosity, the measurements have an experimental uncertainty of  $\pm 1$  to 1.5 log units. On this basis, we suggest that our model may provide a more accurate estimate for this melt's temperature dependent viscosity.

The ability of the model to predict volatile-enriched melts that are independent of the model-calibration process is tested in Fig. A1B. The model reproduces the high-temperature viscosity data available for hydrous (RMSE=0.47) and for F-bearing (RMSE=0.11). The low-temperature (high viscosity) data show more scatter but the predicted values are completely within experimental tolerances. The ability of the multicomponent chemical model to reproduce viscosity measurements on a diverse range of melts that are not in the database used for calibration purposes is an important attribute because it indicates that the model can be extrapolated past the original database.

#### Appendix B. Supplementary data

Supplementary data associated with this article can be found, in the online version, at doi:10.1016/j.epsl.2008.03.038.

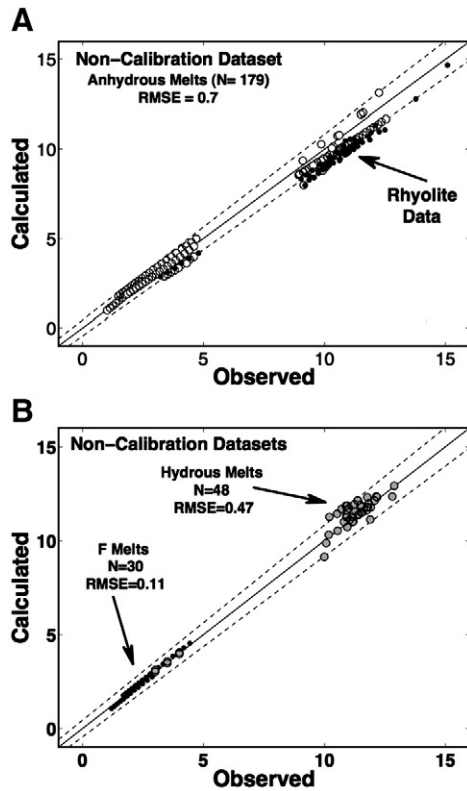


**Fig. A1.** The ability of this model to predict the viscosity of melt compositions not included in the calibration database. Observed values of  $\log \eta$  are compared against calculated values of  $\log \eta$  for: (A) anhydrous ( $N=179$  experiments) melts including a series of high variance measurements on rhyolite melts (Neuville et al., 1993), and (B) hydrous ( $N=48$  experiments) and fluorine bearing ( $N=30$  experiments) melts. Dashed lines indicate  $\pm 5\%$  uncertainty on measured values of  $\log \eta$ .

## References

- Angell, C.A., 1995. Relaxations in Complex Systems (U.S. Department of Commerce National Technical Information Service, ed. K.L. Ngai and G.B. Wright, 1985), pp. 3–11.
- Angell, C.A., 1991. Relaxation in liquids, polymers and plastic crystal-strong/fragile patterns and related problems. *J. Non-Cryst. Solids* 131–133, 13–31.
- Avramov, I., 2007. Pressure and temperature dependence of viscosity of glassforming and of geoscientifically relevant system. *J. Volcanol. Geotherm. Res.* 160, 165–174.
- Bagdassarov, N.S., Dingwell, D.B., 1992. A rheological investigation of vesicular rhyolite. *J. Volcanol. Geotherm. Res.* 50, 307–322.
- Baker, D.R., 1996. Granitic melt viscosities: Empirical and configurational entropy models for their calculation. *Am. Mineral.* 81, 126–134.
- Bottinga, Y., Weill, D., 1972. The viscosity of magmatic silicate liquids: a model for calculation. *Am. J. Sci.* 272, 438–475.
- Bouhifd, A.M., Richet, P., Besson, P., Roskosz, M., Ingrin, J., 2004. Redox state, microstructure and viscosity of a partially crystallized basalt melt. *Earth Planet. Sci. Lett.* 218, 31–44.
- Bourgue, E., Richet, P., 2001. The effect of dissolved CO<sub>2</sub> on the density and viscosity of silicate melts: a preliminary study. *Earth Planet. Sci. Lett.* 193, 57–68.
- Dingwell, D.B., 1991. Redox viscosimetry of some Fe-bearing silicate liquids. *Am. Mineral.* 76, 1560–1562.
- Dingwell, D.B., 1996. Volcanic dilemma: Flow or blow? *Science* 273, 1054–1055.
- Dingwell, D.B., 2006. Transport properties of magmas: Diffusion and rheology. *Elements* 2, 281–286.
- Dingwell, D.B., Hess, K.U., 1998. Melt viscosities in the system Na–Fe–Si–O–F–Cl: Contrasting effects of F and Cl in alkaline melts. *Am. Mineral.* 83, 1016–1021.
- Dingwell, D.B., Webb, S.L., 1989. Structural relaxation on silicate melts and non-Newtonian melt rheology in geologic processes. *Phys. Chem. Miner.* 16, 508–516.
- Dingwell, D.B., Bagdassarov, N.S., Bussod, G.Y., Webb, S.L., 1993. Magma rheology. Experiments at high pressures and application to the earth's mantle. *Mineral. Assoc. Canada Short Course Handbook*, vol. 21, pp. 233–333.
- Dingwell, D.B., Courtial, P., Giordano, D., Nichols, A.R.L., 2004. Viscosity of peridotite liquid. *Earth Planet. Sci. Lett.* 226, 127–138.
- Eyring, H., Henderson, D., Stover, B.J., Eyring, E.M. *Statistical Mechanics and Dynamics*, John Wiley eds, Second edition, NY, 1982. 785 pp (ISBN: 0471370428).
- Fulcher, G.S., 1925. Analysis of recent measurements of the viscosity of glasses. *J. Am. Ceram. Soc.* 8, 339–355.
- Ghiorso, M.S., Sack, R.O., 1995. Chemical mass transfer in magmatic processes. IV. A revised and internally consistent thermodynamic model for the interpolation and extrapolation of liquid–solid equilibria in magmatic systems at elevated temperatures and pressures. *Contrib. Mineral. Petrol.* 119, 197–212.
- Giordano, D., Dingwell, D.B., 2003. Non-Arrhenian multicomponent melt viscosity: A model. *Earth Planet. Sci. Lett.* 208, 337–349.
- Giordano, D., Russell, J.K., 2007. A rheological model for glassforming silicate melts in the systems CAS, MAS, MCAS. *J. Phys. Condens. Matter* 19, 205148.
- Giordano, D., Romano, C., Papale, P., Dingwell, D.B., 2004a. The viscosity of trachytes, and comparison with basalts, phonolites, and rhyolites. *Chem. Geol.* 213, 49–61.
- Giordano, D., Romano, C., Poe, B., Dingwell, D.B., Behrens, H., 2004b. The combined effects of water and fluorine on the viscosity of silicic magmas. *Geochim. Cosmochim. Acta* 68, 5159–5168.
- Giordano, D., Mangicapa, A., Potuzak, M., Russell, J.K., Romano, C., Dingwell, D.B., Di Muro, A., 2006. An expanded non-Arrhenian model for silicate melt viscosity: A treatment for metaluminous, peraluminous and peralkaline melts. *Chem. Geol.* 229, 42–56.
- Goto, A., Taniguchi, H., Kitakaze, A., 2005. Viscosity measurements of hydrous rhyolitic melts using the fiber elongation method. *Bull. Volcanol.* 67, 590–596.
- Greenwood, H.J., 1989. On models and modeling. *Can. Mineral.* 1–14.
- Hess, K.U., Dingwell, D.B., 1996. Viscosities of hydrous leucogranitic melts: A non-Arrhenian model. *Am. Mineral.* 81, 1297–1300.
- Hui, H., Zhang, Y., 2007. Toward a general viscosity equation for natural anhydrous and hydrous silicate melts. *Geochim. Cosmochim. Acta* 71, 403–416.
- Kohn, S.C., 2000. The dissolution mechanisms of water in silicate melts: A synthesis of recent data. *Mineral. Mag.* 64, 389–408.
- Mysen, B.O., 1988. *Structure & Properties of Silicate Melts*. Elsevier, Amsterdam. 354 pp.
- Myuller, R.L., 1955. A valence theory of viscosity and fluidity for high-melting glass-forming materials in the critical temperature range. *Zh. Prikl. Khim.* 28, 1077–1087.
- Neuville, D.R., Courtial, P., Dingwell, D.B., Richet, P., 1993. Thermodynamic and rheological properties of rhyolite and andesite melts. *Contrib. Mineral. Petrol.* 113, 572–581.
- Papale, P., 1999. Strain-induced magma fragmentation in explosive eruptions. *Nature* 397, 425–428.
- Persikov, E.S., 1991. The viscosity of magmatic liquids: Experiment generalized patterns, a model for calculation and prediction, applications. In: Perchuk, L.L., Kushiro, I. (Eds.), *Physical Chemistry of Magmas*, Advances in Physical Chemistry. Springer, Berlin, pp. 1–40.
- Plazek, D.J., Ngai, K.L., 1991. Correlation of polymer segmental chain dynamics with temperature-dependent time-scale shifts. *Macromolecules* 24, 1222–1224.
- Richet, P., Bottinga, Y., 1995. Rheology and configurational entropy of silicate melts. In: Stebbins, J.F., McMillan, P.F., Dingwell, D.B. (Eds.), *Structure, Dynamics and Properties of Silicate Melts*.
- Russell, J.K., Giordano, D., 2005. A model for silicate melt viscosity in the System CaMgSi<sub>2</sub>O<sub>6</sub>–CaAl<sub>2</sub>Si<sub>2</sub>O<sub>8</sub>–NaAlSi<sub>3</sub>O<sub>8</sub>. *Geochim. Cosmochim. Acta* 69, 5333–5349.
- Russell, J.K., Quane, S., 2005. Rheology of welding: Inversion of field constraints. *J. Volcanol. Geotherm. Res.* 142, 173–191.
- Russell, J.K., Giordano, D., Dingwell, D.B., Hess, K.U., 2002. Modelling the non-Arrhenian rheology of silicate melts: Numerical considerations. *Eur. J. Mineral.* 14, 417–427.
- Russell, J.K., Giordano, D., Dingwell, D.B., 2003. High-temperature limits on viscosity of non-Arrhenian silicate melts. *Am. Mineral.* 8, 1390–1394.
- Shaw, H.R., 1972. Viscosities of magmatic silicate liquids: An empirical method of prediction. *Am. J. Sci.* 272, 870–893.
- Sparks, R.S.J., 2004. Dynamics of magma degassing. *Volcanic degassing*, *Geol. Soc. Lond. Spec. Pub.* 213, 5–22.
- Streck, M.J., Gruner, A.L., 1995. Crystallization and welding variations in a widespread ignimbrite sheet; the Rattlesnake Tuff, eastern Oregon, USA. *Bull. Volcanol.* 57, 151–169.
- Toplis, M.J., 1998. Energy barriers to viscous flow and the prediction of glass transition temperatures of molten silicates. *Am. Mineral.* 83, 480–490.
- Scopigno, T., Rocco, G., Sette, F., Monaco, G., 2003. Is the fragility of a liquid embedded in the properties of its glass? *Science* 302, 849–852.
- Vetere, F., Behrens, H., Holtz, F., Neuville, D.R., 2006. Viscosity of andesitic melts – New experimental data and a revised calculation model. *Chem. Geol.* 228, 233–245.
- Vogel, D.H., 1921. Temperaturabhängigkeitsgesetz der Viskosität von Flüssigkeiten. *Phys. Z.* 22, 645–646.
- Whittington, A., Richet, P., Linard, Y., Holtz, F., 2001. The viscosity of hydrous phonolites and trachytes. *Chem. Geol.* 174, 209–223.
- Zimova, M., Webb, S.L., 2006. The combined effects of chlorine and fluorine on the viscosity of aluminosilicate melts. *Geochim. Cosmochim. Acta* 71, 1553–1562.